



# Erasure of nanopores in silicate glasses induced by femtosecond laser irradiation in the Type II regime

Maxime Cavillon<sup>1</sup> · Yitao Wang<sup>1</sup> · Bertrand Poumellec<sup>1</sup> · François Brisset<sup>1</sup> · Matthieu Lancry<sup>1</sup>

Received: 15 June 2020 / Accepted: 7 October 2020 / Published online: 20 October 2020  
© Springer-Verlag GmbH Germany, part of Springer Nature 2020

## Abstract

Optical devices fabricated by femtosecond (fs) laser within the Type II regime are of interest for high temperature applications ( $> 800$  °C). fs-Type II regime is characterized by the formation of self-organized nanogratings, which are composed of regularly spaced porous nanolayers with nanopores having a typical size of a few tens of nm. In this work, we first investigate the evolution of the nanopore size distribution as a function of fs-laser writing speed and pulse energy, as well as a function of annealing temperature after fs-laser irradiation. Then, the thermal stability of such nanopores is numerically investigated through the use of the Rayleigh–Plesset (R–P) equation, and is compared with experimental data. The R–P equation provides insights into the temperature range at which the nanopores would ultimately collapse, serving as a design tool for future high temperature fs-Type II based devices. The key role of glass viscosity and nanopore diameter on the overall thermal stability is also discussed.

**Keywords** Femtosecond laser · Nanogratings · Silicate glasses · Thermal stability

## 1 Introduction

Optical devices capable to withstand and operate at high temperatures ( $> 800$  °C) for a long period of time (e.g., hundreds of hours) are attractive for many applications, including aircraft engine monitoring, fuel bed combustors, long lifetime optical data storage or fiber lasers [1–3]. Within the tools at one’s disposal to fabricate devices in both fiber and bulk glass materials, femtosecond laser-direct writing (FLDW) is particularly interesting. Indeed, FLDW is a versatile technique that enables high peak powers to induce local three-dimensional (3D) modifications inside the glass substrate, due to the nonlinear absorption processes involved during the laser light–matter interaction. One of the unique features of FLDW is the possibility to induce self-organized nanogratings, within the so-called Type II regime [4]. In addition, nanogratings have been reported in a variety of glasses, including silica, germanates, silicates, borosilicates [5, 6].

In silica, these nanogratings can survive beyond 1000 °C for several hours [7], and are composed of regularly spaced porous nanolayers (typically few tens of nm thickness, with a period of about 300 nm). The latter are filled with nanopores having their size and number being a function of the laser parameters as well as the glass material [8]. Upon an increase in temperature, Type II regime laser-induced modifications would be accompanied by changes in the glass structure (e.g., point defects, stress, specific volume) and in the related physical properties (e.g., refractive index, birefringence, light absorption and scattering). Such modifications will ultimately dictate the response and the lifetime of a fabricated optical device (e.g., a grating used as a sensor [2] or a dot used for 5D optical data storage [3]).

Thus, it is critical to understand what are the underlying mechanisms that drive the evolution of these aforementioned modifications at high temperatures. The annealing of fs-laser induced nanogratings yield to some modifications, at different temperature ranges, which have previously been investigated and reported. For instance, the presence of laser induced defects, such as non-bridging oxygen hole centers (NBOHC), fully erased at 600 °C within a few minutes [9]. Additionally, in silica the typically large amount of 3- and 4-membered rings, characteristic of densification and the presence of an intense compressive stress induced by Type

✉ Maxime Cavillon  
maxime.cavillon@universite-paris-saclay.fr

<sup>1</sup> Institut de Chimie Moléculaire et des Matériaux d’Orsay (ICMMO/SP2M/MAP), Université Paris-Saclay, CNRS, 91405 Orsay Cedex, France

II laser irradiation, is found to decrease and to anneal away within the 800–900 °C temperature range [9, 10]. Moreover, the stress field associated with the formation of nanogratings (see for instance Ref. [11]) is typically relaxed slightly below or at the glass transition temperature ( $\sim 1100$  °C for silica) [10, 12, 13]. Ultimately, the fs-induced modifications correspond to a permanently decomposed glass with nanopores embedded inside it [14, 15]. As a note, the presence of defects in the glass, as discussed above, is partly associated with the dissociation of  $\text{SiO}_2$  into  $\text{SiO}_{2(1-x)} + x\text{O}_2$  [14]. The Raman peak intensity, centered at  $1556\text{ cm}^{-1}$  in Ref. [14], is characteristic of free  $\text{O}_2$  inside the glass nanopores [16]. Increasing the temperature in the 300–600 °C range causes bleaching of defects, which would yield a decrease of the  $\text{O}_2$  pressure. The signature of free  $\text{O}_2$  is detected up to  $\sim 600$  °C using Raman spectroscopy (see Fig. 3.14 of Ref. [17]), and agrees well with the aforementioned defect bleaching.

In this work, we first investigate the nanopore size distribution, in silica glass, for different writing conditions (varying scanning speeds and pulse energies), as well as the erasure of the nanopores through heat treatments at different temperatures. Variations in the average nanopore diameter are observed [18]. Following this, the thermal stability of the laser induced nanopores is investigated using the Rayleigh–Plesset (R–P) equation [19], assuming the nanopores to have a spherical shape. In practice, the nanopores can take the form of ellipsoids or more complex shapes [20, 21]. However, this work intends to set the basis for future work to include these difficulties, and therefore, only spherical particles are considered herein.

The role played by both the glass material (including pure silica – Infrasil and PCVD types, Borofloat 33 – composition in mole%: 81% $\text{SiO}_2$ –13%B $_2$ O $_3$ –4%Na $_2$ O/K $_2$ O–2%Al $_2$ O $_3$ , and ULE glass – Ultra Low Expansion and in mole%: 93% $\text{SiO}_2$ –7%TiO $_2$ ) and the initial nanopore

diameter on the overall thermal stability of the fs-induced nanogratings are modeled using the R–P equation, and compared with experimental data. This work is aimed to provide preliminary insights on the ultimate stability of the nanopores present in the glass. This may be used as a means to ease the selection of glass material and laser parameters to enhance thermal stability in future optical designs operating in a high temperature environment.

## 2 Materials and methods

First, the nanopore size distribution within the porous regions is investigated for three different pure silica glass samples (labeled S1, S2 and S3), which are reported in Table 1, along with the different laser irradiation conditions used. For S1 sample the writing speed is varied from  $0.01\text{ mm s}^{-1}$  to  $10\text{ mm s}^{-1}$ . For S2, the pulse energy is varied from  $0.2\text{ }\mu\text{J}$  to  $1.0\text{ }\mu\text{J}$ , and for S3 Type II laser-induced modifications are consecutively annealed for 30 min at 1000 °C, 1100 °C, and 1200 °C. To investigate the nanopores and their size distribution, each sample was cleaved perpendicularly to the laser light polarization direction (for instance see Ref. [1]) and imaged by a scanning electron microscope (FEG–SEM Zeiss Supra 55 VP).

Following the investigation of the nanopore sizes, a numerical approach, using the Rayleigh–Plesset (R–P) equation, is undertaken to simulate the erasure of the nanopores during the thermal annealing. The R–P equation is derived from the Navier–Stokes equation and physically describes the evolution of a spherical bubble inside an incompressible Newtonian fluid. The R–P equation takes the following form [19, 22, 23]:

**Table 1** Glass samples and laser irradiation conditions investigated for nanopore size distribution characterization

Materials	Silica suprasilCG	Silica PCVD	Silica suprasilCG
Sample labelling	S1 <sup>1</sup>	S2	S3
Pulse energy ( $\mu\text{J}$ )	2.0	0.2; 0.4; and 1.0	1.0
Writing speed, $v$ ( $\text{mm s}^{-1}$ ) <sup>2</sup>	0.01; 0.1; 1; 10	0.1	1
Repetition rate, $f$ (kHz)	100	100	100
Number of pulses per $\mu\text{m}$	10,000; 1,000; 100; 10	1,000	1,000
Wavelength (nm)	1030	1030	1030
Pulse duration (fs)	250	300	300
Numerical aperture, NA	0.6	0.6	0.6
Focusing depth ( $\mu\text{m}$ )	–	300	300
Configuration <sup>3</sup>	–	//	//

<sup>1</sup>This sample is the same as in Ref.[8]

<sup>2</sup>Varying the laser writing speed  $v$  with a constant repetition rate  $f$  is equivalent to changing the pulse density  $v/f$ , or the “number of pulses per  $\mu\text{m}$ ” as defined in the table

<sup>3</sup>// or  $\perp$ : Laser polarization parallel (//) or perpendicular ( $\perp$ ) to the writing direction

$$\frac{\Delta P}{\rho} = R_{\text{pore}} \frac{d^2 R_{\text{pore}}}{dt^2} + \frac{3}{2} \left( \frac{dR_{\text{pore}}}{dt} \right)^2 + \frac{4\eta(T)}{\rho R_{\text{pore}}} \frac{dR_{\text{pore}}}{dt} + \frac{2S}{\rho R_{\text{pore}}}. \quad (1)$$

In this equation,  $\Delta P$  is the pressure difference (in Pa) between the inside of the nanopore (supposed spherical) and far away from it,  $\rho$  is the glass density (in  $\text{kg m}^{-3}$ ),  $R_{\text{pore}}$  the radius (in m) of the spherical nanopore,  $t$  the time (in s),  $\eta(T)$  the glass viscosity (in Pa.s), and  $S$  is the surface energy (around  $0.3 \text{ J m}^{-2}$  for silica [24]). Both  $\rho$  and  $S$  are set independent to the temperature for sake of simplicity. The viscosity is extrapolated from glass manufacturer datasheets (Borofloat33, SuprasilCG, Infrasil and PCVD) and from Ref. [8] for ULE glass, using a Vogel–Tammann–Fulcher (VTF) law in the form  $\log(\eta) = A + B/(T - T_0)$ . Initial conditions are  $R_{\text{pore}}(\text{at } t=0) = R_0$  and  $dR_{\text{pore}}/dt(\text{at } t=0) = 0$ . The equation is solved numerically using an ordinary differential equation (ODE) built-in solver from Matlab software. This work only intends to provide preliminary understandings on the ultimate stability of nanopores using the R–P equation. Therefore, several assumptions and simplifications are made. First, we set  $\Delta P = 0$ , as the decrease in  $\text{O}_2$  concentration inside the nanopore, due to bleaching of defects as described in the introduction below  $600 \text{ }^\circ\text{C}$ . Indeed, and as already described in the introduction section, the oxygen inside the nanopore is associated with formation of defects, and the oxygen is inserted back into the structure below  $600 \text{ }^\circ\text{C}$  (and, therefore, without long distance diffusion). It would result in a rather small  $\text{O}_2$  pressure, which will be subsequently neglected throughout the paper. The R–P equation is used to compute the nanopore size evolution for different glasses, including pure silica (PCVD, Infrasil301), Borofloat33 and ULE, which have been reported in Ref. [8]. In these experiments, the thermal stability of Type II nanostructures is investigated through step isochronal measurements ( $\Delta t = 30 \text{ min}$ ,  $\Delta T$  typ.  $25 \text{ }^\circ\text{C}$  or  $50 \text{ }^\circ\text{C}$ ) and by monitoring the retardance induced by the birefringent nanogratings. The Retardance ( $R$ ) is defined as the product of the Birefringence ( $B$ ) with the length ( $L$ ) of the birefringent object ( $R = B \times L$ ). In Ref. [8], the aforementioned  $R(\Delta t, T)$  values measured at room temperature after each annealing step are normalized relative to the initial (not annealed)  $R(t=0, 20 \text{ }^\circ\text{C})$  value. In this work, the experimental data are normalized with respect to the  $R$  value at the temperature above which the retardance experiences a steep decay rate (e.g.,  $T = 1225 \text{ }^\circ\text{C}$  for Infrasil301 in Fig. 5a in Ref. [8]). The latter normalization enables to investigate only the last step of nanograting erasure.

To compare the computed results from the R–P equation with the experimental normalized  $R$  values, the nanopore diameter (from R–P equation) is converted to a normalized retardance value following the procedure described below. First, we calculate the average refractive index of the porous nanolayer ( $n_{pl}$ ) using the Maxwell–Garnet equation [25]:

$$n_{pl} = \sqrt{\frac{n_G^2 + \frac{(1+2FF)}{3}(n_{\text{pore}}^2 - n_G^2)}{n_G^2 + \frac{(1-FF)}{3}(n_{\text{pore}}^2 - n_G^2)}}}. \quad (2)$$

In the above equation,  $n_G$  is the glass refractive index (taken as 1.4599, i.e., index of silica at  $551 \text{ nm}$ ), which is assumed independent of temperature (small  $dn/dT$  of  $\sim 10 \times 10^{-6} \text{ K}^{-1}$  [26]). This value is taken equal both inside the porous nanoplanes (i.e., around the nanopores) and between the porous nanoplanes. This simplification is acceptable in the conditions of this work, as we principally focus on the erasure of the nanopores for temperatures at, or above, the glass transition temperatures of the glass materials investigated. Therefore, the contributions to the refractive index due for instance to the presence of a stress field (see for example Fig. 5a in Ref. [13]), or a permanent densification of the glass, are annealed away (Refs. [17, 27]).  $FF$  is the filling factor, defined here as the relative volume taken by the nanopores per unit volume of porous nanolayer (labeled  $V$ ), and  $n_{\text{pore}}$  is the nanopore refractive index, taken equal to 1. The filling factor is related to the averaged nanopore radius ( $R_{\text{pore}}$ ) through the following equation:

$$FF = N \frac{4\pi R_{\text{pore}}^3}{3V}. \quad (3)$$

Here,  $N$  is the number of nanopores (with an averaged nanopore radius  $R_{\text{pore}}$ ) per unit volume  $V$  of porous nanolayer. A 2D filling factor, corresponding to the area taken by the nanopores per unit surface of porous nanolayer, can be determined from SEM micrographs and is usually in the order of 20–40% [18]. The latter (labeled  $FF_{2D}$ ) will be used in Sect. 3. When discussing the normalized retardance in Sect. 3.3, the  $FF$  defined in Eq. 3 is computed. Additionally, in this work, the refractive index of the glass between the porous nanolayers is set equal to  $n_G$  as in Ref. [18]. Hence, the birefringence  $B = n_o - n_e$ , where  $n_o$  and  $n_e$  are the refractive indices of the ordinary and extraordinary axes, respectively, is calculated from [7, 18]:

$$B = n_o - n_e = \sqrt{\left[1 - \frac{\delta}{\Lambda}\right] n_G^2 + \frac{\delta}{\Lambda} n_{pl}^2} - \left[ \sqrt{\frac{\left[1 - \frac{\delta}{\Lambda}\right] + \frac{\delta}{\Lambda}}{n_G^2} + \frac{\delta}{\Lambda} n_{pl}^2}} \right]^{-1}. \quad (4)$$

Here,  $\Lambda$  is the average spacing between nanolayers,  $\delta$  is the porous nanolayer thickness, and  $(\Lambda - \delta)$  is the interlayer thickness. Finally, the linear retardance can be calculated using the expression  $R = B \times L$  as defined above.

### 3 Results

#### 3.1 Impact of laser writing conditions on the evolution of nanopore size and distribution

The impact of the writing speed in the nanopore morphology is depicted in Fig. 1, where SEM micrographs, nanopore size distribution, 2D filling factor and averaged nanopore diameter as a function of writing speed, are displayed (using Sample S1). We observed that the average nanopore diameter increases when writing speed increases (from 53 to 77 nm from 0.01 mm s<sup>-1</sup> to 10 mm s<sup>-1</sup>, respectively, corresponding to a ~ 45% increase). As the writing speed

increases, the spread of the nanopore diameter distribution also becomes larger (e.g., standard deviation is increased from 13 to 34 nm between 0.01 mm s<sup>-1</sup> and 10 mm s<sup>-1</sup>). While the average nanopore size is increased when speed is increased, the 2D filling factor comparatively decreases. The evolution of FF<sub>2D</sub> observed in Fig. 1 is qualitatively in agreement with retardance values reported in Ref. [8]. However, it is worth pointing out that other contributions factor into the measured retardance value, such as laser track length, porous nanolayer thickness or periodicity.

The evolution of the nanopore size and distribution, as presented in Fig. 1 with respect to varying writing speed conditions, is now investigated through the variation of the laser pulse energy, everything else being set constant (using Sample S2). The results are reported in Fig. 2. An increase

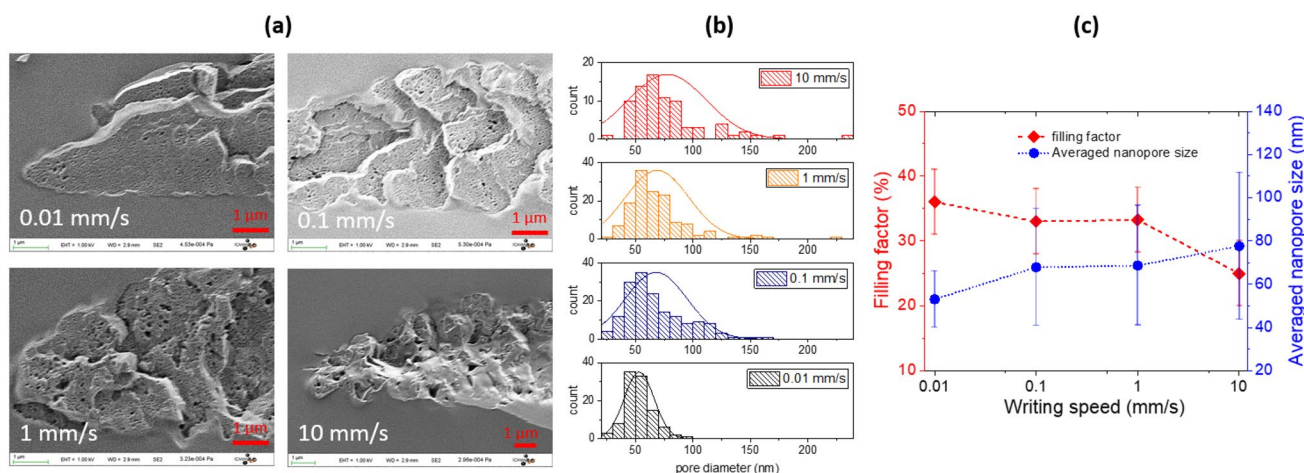


**Fig. 1** Effect of the writing speed on nanopore size, distribution and filling factor, using Sample S1. **a** scanning electron micrographs of the porous regions for different writing speeds; **b** nanopore diameter

distributions with respect to the writing speed; **c** evolution of the 2D porosity filling factor and the average nanopore diameter as a function of writing speed. The lines only serve as a guide-to-the-eye

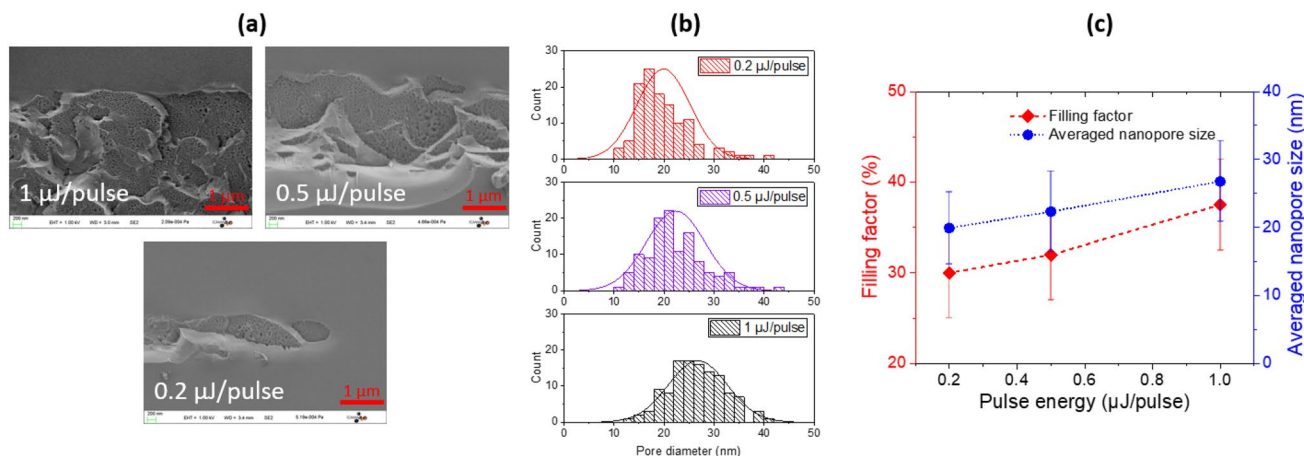


**Fig. 2** Effect of the laser pulse energy on nanopore size, distribution and filling factor, using Sample S2. **a** scanning electron micrographs of the porous regions for different pulse energies; **b** nanopore diam-

eter distributions with respect to pulse energy; **c** evolution of the 2D porosity filling factor and the average nanopore diameter as a function of pulse energy. The lines only serve as a guide-to-the-eye

of the pulse energy is associated with an increase in the nanopore diameter, which exhibits an almost linear rate within the investigated interval ( $\sim 8.6$  nm diameter increase per  $\mu\text{J}$ ). There is almost no evolution of the standard deviation (5.3 nm and 5.9 nm for 0.2  $\mu\text{J}$  and 1.0  $\mu\text{J}$ , respectively). However, as opposed to the results from Fig. 1a, the increase in energy is associated with an increase of the filling factor, and is in agreement with a higher retardance value (for instance in Ref. [28]).

### 3.2 Experimental observation of the decrease in nanopore size and distribution during annealing process

The evolution of the nanopore morphology and size distribution as a function of annealing temperature (for isochronal time steps  $\Delta t$  of 30 min, and using sample S3) is reported in Fig. 3. In this experiment, we observe that the nanopore diameter decreases first as the temperature increases, but appears to plateau at the highest temperature. This effect can be interpreted from the results obtained by the R–P equation, and is discussed in the following section. On the other hand, we observed a diminution of  $FF_{2D}$  that is characteristic of a decrease in the birefringence response (hence the measured retardance). Other SEM micrograph analysis, not presented here, also showed that both thickness of planes and spacing between planes were independent of temperature.

### 3.3 Simulation study of the decrease in nanopore size in annealing process by the Rayleigh–Plesset equation

Thermal stability of Type II nanogratings inscribed in various glasses (silica and silicate glasses) were investigated

and reported in Ref. [8], using step isochronal annealing experiments ( $\Delta t = 30$  min,  $\Delta T = 25$  °C). These data are displayed in Fig. 4, but normalized relative to the sharp retardance decrease at the highest annealing temperature values that we hypothesized here to be characteristic of the nanopore erasure. It is worth pointing out that in order for each data point to be independent to the other, the criterion  $(\Delta t \times k_0)^{-\Delta T/T_{\max}} \ll 1$  must be fulfilled [29] (with  $k_0$  estimated to be around  $5 \times 10^5$  to  $5 \times 10^7$   $\text{s}^{-1}$  for nanogratings erasure in silica [30]). In this work, this criterion is not satisfied, and therefore, the thermal stability in this condition is expected to be slightly underestimated with respect

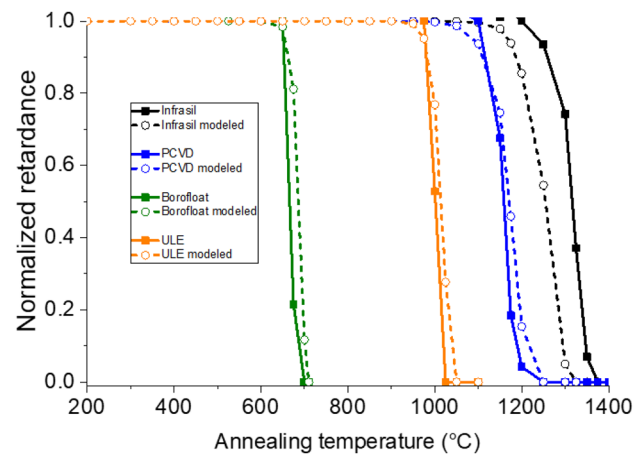


**Fig. 4** Evolution of the normalized retardance during step isochronal annealing experiments for various glasses (taken and re-normalized from Ref. [8]) compared with the Rayleigh–Plesset (R–P) equation used to simulate the nanopores’ erasure. Conditions used in the simulation:  $\Delta P = 0$  Pa;  $S = 0.3$   $\text{J m}^{-2}$ ;  $\rho = 2200$   $\text{kg m}^{-3}$ ; Initial nanopore radius used during calculation:  $R(t=0) = 25$  nm;  $\eta(T)$  fitted using a VTF law for each glass (Infrasil, PCVD, Borofloat33, and ULE)

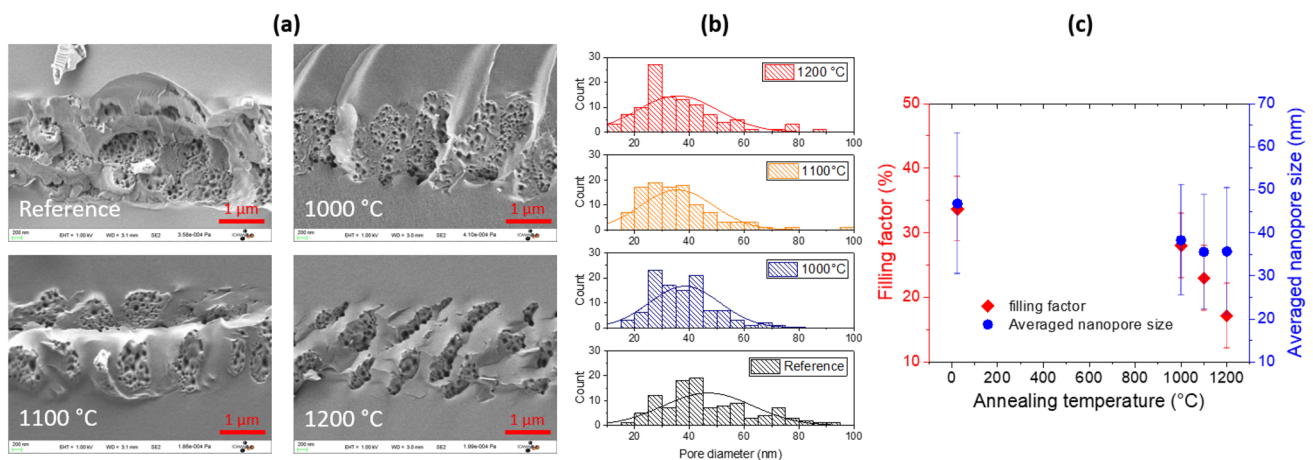
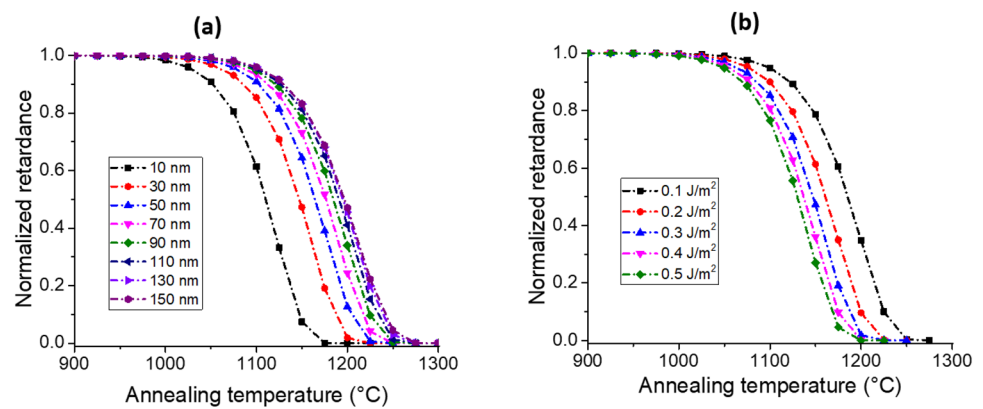


**Fig. 3** Effect of thermal annealing on nanopore size, distribution and filling factor, using Sample S3. **a** scanning electron micrographs of the porous regions for different annealing temperatures ( $\Delta t = 30$  min);

**b** nanopore diameter distributions with respect to annealing temperature; **c** evolution of the 2D porosity filling factor and the average nanopore diameter as a function of annealing temperature

**Fig. 5** Evolution of the Retardance (only taking into account the evolution of the nanopores) for step isochronal annealing experiments ( $\Delta t = 30$  min,  $\Delta T = 25$  °C) for SuprasilCG glass simulated by Rayleigh–Plesset (R–P) equations. **a** Effect of initial nanopore diameter (from 10 to 150 nm), with a constant value of  $S = 0.3$  J m<sup>-2</sup>. **b** Effect of surface energy  $S$  (from 0.1 to 0.5 J m<sup>-2</sup>), with a constant value of  $R(t=0) = 15$  nm



to a stability curve having independent data points. In this paper only the final erasure step of the measured retardance  $R(\Delta t, T)$  is investigated. Following the same experimental conditions as in the experiment, the Rayleigh–Plesset (R–P) equation was used to simulate the nanopore erasure, and the evolution of the retardance was calculated based the nanopore diameter, the filling factor FF and using the form birefringence equations (Eqs. 2, 3, and 4) shown above. Here we assume that the nanolayers thickness ( $\delta$ ), the average spacing ( $A$ ), and the interlayer thickness ( $A - \delta$ ), and the laser track length ( $L$ ) did not change with the annealing steps. The comparison between experimental data and the simulated data (using R–P equation) are reported in Fig. 4. It is worth pointing out that the R–P equation computed here is for a single initial nanopore diameter. However, as was previously discussed, the nanopore diameter is distributed in a fairly wide interval, depending on the laser writing conditions but also with the chemical composition [6, 31]. However, as a first approximation, one can note that evolution of the simulated retardance, related to the erasure of the nanopores using the R–P equation, agrees rather well with the experimental data, even when the viscosity dynamics is found to vary by several order of magnitudes with respect to temperature for the studied glasses. This is indicative that viscosity (and its temperature dependence) is a first order property in the erasure mechanism of nanogratings and their associated form birefringence in a high temperature regime.

The effects of both nanopore diameter and surface energy  $S$  (from R–P equation) are investigated and reported in Fig. 5a and b. As the initial nanopore diameter is increased or the glass surface energy is decreased, the annealing curves shift to higher temperatures. With a 100 nm nanopore diameter change, thermal stability curve is expected to shift by  $\sim 100$  °C (for a normalized retardance value of 0.5). In contrast, the surface energy plays a less significant role in the process, since a large change of surface energy ( $\Delta S = 0.4$  J m<sup>-2</sup>) shifts only by  $\sim 50$  °C the annealing curves. The discrepancy between the experimental data and the model observed in Fig. 4 for the Infrasil301 could

potentially be attributed to a variation of surface energy, although further investigations would be necessary to verify this hypothesis.

## 4 Discussion

In the previous section we have shown that the thermal stability of nanogratings (evaluated through optical retardance measurements) induced by IR fs-laser (so called Type II regime) is not only a function of the silicate glass chemical composition but also of the nanogratings morphology. The use of various laser-writing parameters, including writing speed (hence linear pulse density) and pulse energy, directly influence the distribution and the size of the nanopores within the porous nanolayers. A direct consequence of this is the change in the thermal stability of optical devices fabricated by Type II fs-laser writing. As an example, the average refractive index changes along the “fringes” of a Type II fiber Bragg grating (such as the ones in Ref. [2]) would be equal to  $(n_e + n_o)/2$ . In contrast polarizing based devices like radial–azimuthal polarization converter [32], achromatic polarization rotator [33], fs-laser-induced waveplates [13, 34] or 5D “eternal” optical memories [3] are based on the optical retardance amplitude and thus proportional to  $(n_e - n_o)$ . Hence, the optical response of these devices at high temperatures would be related to the magnitude of birefringence induced by the overall porous structure, and among which the nanopore size plays an important role.

In addition, the chemical composition of the glass material has a critical role in the erasure of the nanopores, as its viscosity behavior is found to principally dictate the overall nanopore erasure, as shown from the results using R–P equation. For instance, low OH and Cl impurity-containing materials, such as Infrasil301 silica, present high viscosity at high temperatures, which is expected to promote thermal stability of the nanopores. The differences observed in optical properties, here in term of linear birefringence, are in

fairly good agreement between experimental and simulated data using the R–P equation as shown in Fig. 4.

From Fig. 1, the average nanopore diameter increases from 53 to 77 nm between low and high writing speeds ( $0.01\text{--}10\text{ mm s}^{-1}$ ), and the steep decay of the associated isochronal annealing curves is shifted by  $\sim 15\text{ }^\circ\text{C}$  to higher temperatures (Ref. [8]). Using the R–P equation with the experimental conditions described in the same reference, a shift of  $\sim 15\text{ }^\circ\text{C}$  is also predicted.

In Fig. 3c, we observe that, as the irradiated glass is progressively annealed, the nanogratings filling factor  $FF$  decreases, while the averaged nanopore size remains nearly constant. This can be explained on the basis of the R–P equation, where we observe that small nanopores being erased more quickly than the larger ones (see Fig. 5a). As a result, the fully erased small nanopores are not included in the counting to determine the average nanopore diameter. This has an effect of shifting up the average nanopore diameter to larger values. However, the filling factor still decreases as nanopores are progressively erased, which are in agreement with the observation of a decrease in retardance. On a more speculative note and based on results from Fig. 5a and 5b, a possible way to further promote thermal stability could be by minimizing the glass surface energy.

As was mentioned in the introduction, it is worth pointing out that the shape of the nanopore is more ellipsoidal than spherical, as was brought to evidence in Ref. [20] using small angle X-ray scattering (SAXS) measurements. In our conditions and to reveal the porosity of the nanopore layers, the sample are cleaved along the short axis direction and placed under an SEM for observation. But for such geometry (ellipsoid nanopores) the limiting factor of the erasure kinetic is controlled by the short axis of the nanopore. Although the shape of the annealing curve is expected to be slightly modified (and mostly at the highest temperatures), using an ellipsoidal geometry to model the dynamics of the nanopore erasure should not be drastically different with respect to a spherical geometry. Finally, on this matter is it possible to expect the ellipsoids to round up during the annealing to minimize their surface tension.

Type III regime, associated with the formation of nanovoids (typically in the 100 nm to 1  $\mu\text{m}$  diameter range [35–37]), is known to be slightly more stable than type II nanogratings, provided that associated stress and densified shell surrounding the nanovoids can be stabilized. From this work, the larger size of the nanopores is expected to be a principal contributor to this higher thermal stability. Hence, in the realm of high thermal stability devices, one would want to maximize the nanopore diameter. Additionally, a single void structural modification induced by femtosecond laser may be advantageous over nanopores as one would not have to take into account a nanopore size distribution, which may ease thermal stability predictions.

Finally, the viscous behavior of the glass material will ultimately set the upper limit of the thermal stability of the device. Hence the current interest is to develop high viscosity glasses and optical fibers [1, 38].

## 5 Conclusions

In this work, the effect of glass composition and laser parameters upon fs-laser direct writing in the Type II regime (formation of nanogratings), are reported in silica and silicate glasses. The evolution of nanopore diameter as a function of laser writing speed, pulse energy, and temperature (through step isochronal annealing) is investigated and discussed. The Rayleigh–Plesset (R–P) equation is then used to compute the collapse of such nanopores as a function of glass chemical composition and with varying initial nanopore diameters or surface energy values. The R–P equation shed light on the major role played by the temperature dependence of the glass viscosity on the thermal stability of fs-induced Type II modifications. Consequently, it is not only the glass annealing temperature ( $T_a$ ) but rather the viscous behavior of the glass over a temperature range (between  $T_a$  and the softening temperature  $T_{\text{soft}}$ ) that is the major parameter driving the erasure of the nanogratings and their related form birefringence. This viscous behavior is also expected to have an impact on nanogratings formation inside a glass. The initial nanopore diameter is also found to play a significant role in the overall thermal stability of the fs-laser induced modified region. On a final note, this work aims to serve as a roadmap for the development of components stable at high temperatures, by mean of both glass property tailoring (e.g., viscosity, surface energy) and the mastering of laser-induced structural modifications (such as the formation of large nanopores or voids). Future work will involve the implementation of ellipsoid nanopores in the model, along with a size distribution, as well as the injection of densified zones (together with their own thermal stability) within the interlayers.

**Funding** The authors would like to acknowledge the following institutions for funding their research: Agence Nationale pour la Recherche, FLAG/IR project, grant number ANR-18-CE08-0004-01 and CNRS Défi Instrumentation aux Limites, Ultrabragg project.

**Data availability** Not applicable.

**Code availability** Not applicable.

## Compliance with ethical standards

**Conflict of interest** The authors declare no conflict of interest.

## References

- M. Cavillon, M. Lancry, B. Poumellec et al., Overview of high temperature fibre Bragg gratings and potential improvement using highly doped aluminosilicate glass optical fibres. *J. Phys. Photonics* **1**, 042001 (2019). <https://doi.org/10.1088/2515-7647/ab382f>
- S.J. Mihailov, D. Grobncic, C. Hnatovsky et al., Extreme environment sensing using femtosecond laser-inscribed fiber bragg gratings. *Sensors* (2017). <https://doi.org/10.3390/s17122909>
- J. Zhang, M. Gecevičius, M. Beresna, P.G. Kazansky, Seemingly unlimited lifetime data storage in nanostructured glass. *Phys. Rev. Lett.* **112**, 1–5 (2014). <https://doi.org/10.1103/PhysRevLett.112.033901>
- Y. Shimotsuma, P.G. Kazansky, J. Qiu, K. Hirao, Self-organized nanogratings in glass irradiated by ultrashort light pulses. *Phys. Rev. Lett.* **91**, 247405 (2003). <https://doi.org/10.1103/PhysRevLett.91.247405>
- S. Richter, C. Miese, S. Döring et al., Laser induced nanogratings beyond fused silica-periodic nanostructures in borosilicate glasses and ULE™. *Opt. Mater. Express* **3**, 1161–1166 (2013). <https://doi.org/10.1364/OME.3.001161>
- M. Lancry, F. Zimmermann, R. Desmarchelier et al., Nanogratings formation in multicomponent silicate glasses. *Appl. Phys. B Lasers Opt.* **122**, 1–8 (2016). <https://doi.org/10.1007/s00340-016-6337-8>
- E. Bricchi, P.G. Kazansky, Extraordinary stability of anisotropic femtosecond direct-written structures embedded in silica glass. *Appl. Phys. Lett.* **88**, 2–4 (2006). <https://doi.org/10.1063/1.2185587>
- S.-E. Wei, Y. Wang, H. Yao et al., Thermal stability of type II modifications by IR femtosecond laser in silica-based glasses. *Sensors* **20**, 1–14 (2020). <https://doi.org/10.3390/s20030762>
- J.J. Witcher, W.J. Reichman, L.B. Fletcher et al., Thermal annealing of femtosecond laser written structures in silica glass. *Opt. Mater. Express* **3**, 502–510 (2013). <https://doi.org/10.1364/OME.3.000502>
- J. Lu, M. Yang, D.N. Wang et al., Fiber Bragg gratings with enhanced thermal stability by residual stress relaxation. *Opt. Express* **17**, 19785–19790 (2009). <https://doi.org/10.1364/oe.17.019785>
- R.R. Thomson, P. Gillet, S. Mukherjee et al., Stress-state manipulation in fused silica via femtosecond laser irradiation. *Optica* **3**, 1285 (2016). <https://doi.org/10.1364/optica.3.001285>
- V.R. Bhardwaj, P.B. Corkum, D.M. Rayner et al., Stress in femtosecond-laser-written waveguides in fused silica. *Opt. Lett.* **29**, 1312–1314 (2004). <https://doi.org/10.1364/OL.29.001312>
- J. Tian, H. Yao, M. Cavillon et al., A comparison between nanogratings-based and stress-engineered waveplates written by femtosecond laser in silica. *Micromachines* **11**, 1–11 (2020). <https://doi.org/10.3390/mi11020131>
- M. Lancry, B. Poumellec, J. Canning et al., Ultrafast nanoporous silica formation driven by femtosecond laser irradiation. *Laser Photonics Rev.* **7**, 953–962 (2013). <https://doi.org/10.1002/lpor.201300043>
- J. Canning, M. Lancry, K. Cook et al., Anatomy of a femtosecond laser processed silica waveguide. *Opt. Mater. Express* **1**, 998–1008 (2011). <https://doi.org/10.1364/ome.1.000998>
- A.J. Berger, Y. Wang, D.M. Sammeth et al., Aqueous dissolved gas measurements using near-infrared raman spectroscopy. *Appl. Spectrosc.* **49**, 1164–1169 (1995). <https://doi.org/10.1366/0003702953965047>
- F. Zimmermann, *Ultrashort Pulse Induced Nanostructures in Transparent Materials* (Friedrich-Schiller-Universität, Jena, 2017)
- R. Desmarchelier, B. Poumellec, F. Brisset et al., In the heart of femtosecond laser induced nanogratings : From porous nanoplanes to form birefringence. *World J. Nano Sci. Eng.* **5**, 115–125 (2015). <https://doi.org/10.4236/wjnse.2015.54014>
- A. Rudenko, J.P. Colombier, T.E. Itina, Nanopore-mediated ultrashort laser-induced formation and erasure of volume nanogratings in glass. *Phys. Chem. Chem. Phys.* **20**, 5887–5899 (2018). <https://doi.org/10.1039/c7cp07603g>
- S. Richter, A. Plech, M. Steinert et al., On the fundamental structure of femtosecond laser-induced nanogratings. *Laser Photonics Rev.* **6**, 787–792 (2012). <https://doi.org/10.1002/lpor.201200048>
- M. Sakakura, Y. Lei, L. Wang et al., Ultralow-loss geometric phase and polarization shaping by ultrafast laser writing in silica glass. *Light Sci. Appl.* **9**, 1–10 (2020). <https://doi.org/10.1038/s41377-020-0250-y>
- M.S. Plesset, The dynamics of cavitation bubbles. *J. Appl. Mech.* **16**, 277–282 (1949). <https://doi.org/10.1080/15435075.2018.1431546>
- C.E. Brennen, *Cavitation and Bubble Dynamics* (Oxford University Press, Oxford, 1995)
- K. Boyd, H. Ebdorff-Heidepriem, T.M. Monro, J. Munch, Surface tension and viscosity measurement of optical glasses using a scanning CO2 laser. *Opt. Mater. Express* **2**, 1101–1110 (2012). <https://doi.org/10.1364/ome.2.001101>
- V.A. Markel, Introduction to the Maxwell Garnett approximation: Tutorial. *J. Opt. Soc. Am. A* **33**, 1244–1256 (2016). <https://doi.org/10.1364/JOSAA.33.001244>
- M.J. Weber, *Handbook of Optical Materials* (CRC Press, London, 2003)
- F. Zhang, Y. Yu, C. Cheng et al., Wavelength response and thermal stability of embedded nanograting structure light attenuator fabricated by direct femtosecond laser writing. *Appl. Phys. B Lasers Opt.* **117**, 53–58 (2014). <https://doi.org/10.1007/s00340-014-5797-y>
- M. Lancry, J. Canning, K. Cook et al., Nanoscale femtosecond laser milling and control of nanoporosity in the normal and anomalous regimes of GeO<sub>2</sub>-SiO<sub>2</sub> glasses. *Opt. Mater. Express* **6**, 321 (2016). <https://doi.org/10.1364/OME.6.000321>
- B. Poumellec, M. Lancry, Kinetics of thermally activated physical processes in disordered media. *Fibers* **3**, 206–252 (2015). <https://doi.org/10.3390/fib3030206>
- M. Gecevičius, *Polarization Sensitive Optical Elements by Ultrafast Laser Nanostructuring of Glass* (University of Southampton, Southampton, 2015)
- F. Zimmermann, M. Lancry, A. Plech et al., Femtosecond laser written nanostructures in Ge-doped glasses. *Opt. Lett.* **41**, 1161–1164 (2016). <https://doi.org/10.1364/ol.41.001161>
- M. Beresna, M. Gecevičius, P.G. Kazansky, T. Gertus, Radially polarized optical vortex converter created by femtosecond laser nanostructuring of glass. *Appl. Phys. Lett.* **98**, 1–4 (2011). <https://doi.org/10.1063/1.3590716>
- R. Desmarchelier, M. Lancry, M. Gecevičius et al., Achromatic polarization rotator imprinted by ultrafast laser nanostructuring in glass. *Appl. Phys. Lett.* **107**, 181111 (2015). <https://doi.org/10.1063/1.4934866>
- M. Gecevičius, M. Beresna, P.G. Kazansky, Polarization sensitive camera by femtosecond laser nanostructuring. *Opt. Lett.* **38**, 4096–4099 (2013). <https://doi.org/10.1364/ol.38.004096>
- R.J. Williams, R.G. Krämer, S. Nolte et al., Detuning in apodized point-by-point fiber Bragg gratings: insights into the grating morphology. *Opt. Express* **21**, 26854–26867 (2013). <https://doi.org/10.1364/oe.21.026854>
- E.N. Glezer, M. Milosavljevic, L. Huang et al., 3-D optical storage inside transparent materials. *Opt. Lett.* **21**, 2023–2026 (1996)



37. E.G. Gamaly, S. Juodkazis, K. Nishimura et al., Laser-matter interaction in the bulk of a transparent solid: Confined micro-explosion and void formation. *Phys. Rev. B Condens. Matter Mater. Phys.* **73**, 1–15 (2006). <https://doi.org/10.1103/PhysRevB.73.214101>
38. Y. Wang, S. Wei, R.C. Yuta et al., Femtosecond laser direct writing in  $\text{SiO}_2$ - $\text{Al}_2\text{O}_3$  binary glasses and thermal stability of Type II permanent modifications. *J. Am. Ceram. Soc.* (2020). <https://doi.org/10.1111/jace.17164>

**Publisher's Note** Springer Nature remains neutral with regard to jurisdictional claims in published maps and institutional affiliations.